Solving Coupled Channel Differential Equation with the R-Matrix Method Embedded on a Lagrange Mesh: An Application on ^{37}Mg

A DISSERTATION REPORT

submitted in partial fulfillment

of the requirement for the degree

of

Master of Science

in

Physics

submitted by

Anil Kumar

(Enrollment Number: 14615002)

under the supervision of

Dr. Rajdeep Chatterjee

Associate Professor

Department of Physics

Indian Institute of Technology Roorkee

Roorkee - 247667, India

May 2016

Candidate's Declaration

I hereby declare that the dissertation titled **"Solving Coupled Channel Differential Equation with the R-Matrix Method Embedded on a Lagrange Mesh: An Application on ^{37}Mg"** in partial fulfilment of the requirements for the Degree of **M.Sc.(Physics)** and submitted in the **Department of Physics, Indian Institute of Technology Roorkee**, is a report on Solving Coupled Channel Differential Equation with the R-Matrix Method Embedded on a Lagrange Mesh: An Application on ^{37}Mg. This work has been carried out from July 2015 to May 2016 under the supervision of **Dr. Rajdeep Chatterjee**, Associate Professor, Department of Physics, Indian Institute of Technology Roorkee.

I have not submitted this work for the award of any other degree of this or any other institute.

Date:

Place:

Anil Kumar

Enrollment Number: 14615002

M.Sc.(Physics)

This is to certify that the above statement made by the candidate is correct to the best of my knowledge.

Dr. Rajdeep Chatterjee

Associate Professor

Department of Physics

Indian Institute of Technology Roorkee

Roorkee India

i

Acknowledgment

I would like to take this opportunity to express my sincere gratitude to my supervisor **Dr. Rajdeep Chatterjee**, Department of Physics, IIT Roorkee, who gave all possible support and encouragement right from the preliminary stage till completion of this work.

I owe my deep sense of gratitude to the Department of Physics, IIT Roorkee, for providing me infrastructural facilities to complete this dissertation successfully.

(Anil Kumar)
M.Sc. IInd year
Physics
Enrollment No: 14615002
IIT Roorkee, Roorkee

Abstract

The R-matrix Method embedded on a Lagrange Mesh is a very powerful Quantum Mechanical tool which can be used to solve the Coupled Channels Differential Equations. In this report, we have presented the R-matrix approach for calculation of bound state energies for various non-deformed and deformed potentials. The Lagrange mesh technique requires calculation of potential matrix element at just Lagrange points which reduces the computation requirement. The results obtained from R-matrix method are compared with the results of other approaches. In this report, the R-matrix method is mainly applied to the Coupled Channel Radial Schroedinger Equation for ^{37}Mg which contains deformed Wood-Saxon potential.

Contents

Chapter 1

Introduction

Introduction

The aim of this project is to develop an algorithm to solve coupled channel inhomogeneous Schrödinger Equation using R-Matrix method with Lagrange Mesh Technique. We are considering the following type of radial Schrödinger Equation at energy E:

$$(T_c - E)u_c + \sum_{c'} V_{cc'} u_{c'} = 0 \tag{1.1}$$

where $V_{cc'}$ is the coupled channel potential which also includes possible centrifugal term $\hbar^2 l_c(l_c + 1)/2\mu_c r^2$ with l_c as the orbital angular momentum of channel c. T_c is the kinetic energy term:

$$T_c = -\frac{\hbar^2}{2\mu_c}\frac{d^2}{dr^2} \tag{1.2}$$

Exotic Nuclei

The stable nuclei have been studied in very detail for a long time, but they are less than 10 % of total possible nuclei. Most of the nuclei are comparatively less stable and decay in very short duration that their properties and structure are not entirely understood. With the development of technology, it has become possible to synthesize and study relatively loosely bound nuclei.

The number of protons and neutrons tends to remain equal in lighter nuclei and result in the most stable nuclei. With the increase in the number of protons, the Coulomb repulsion among protons increase which demands more neutrons than protons to form stable nuclei. Thus, the heavier nuclei have more neutrons than protons. The plot of nuclei on the graph with the x-axis as the number of neutrons and y-axis as the number of protons clear shows that the stable nuclei lie along a straight line. This is also called the island of stability.

There are many nuclei which do not lie on the island of stability. These nuclei having the excess of either neutrons or protons are called **exotic nuclei**. The exotic nuclei are comparatively less stable and tend to stabilize through beta decay. The exotic nuclei having the excess of protons undergo positive beta decay and convert a proton into neutron while exotic nuclei with the excess of neutron undergo negative beta decay and changes a neutron into a proton.

The neutron or proton separation energies of exotic nuclei are very low and eventually become zero when they are very far from the line of stability. This region is called the drip line. The line containing those nuclei in which no more neutron (proton) can be added, is called neutron (proton) drip line. The proton drip line is closer to the line of stability because the proton removal energy is lower than neutron removal energy due to Coulomb repulsion.

Most of the nuclei along the drip line are difficult to synthesis and decay very rapidly, but they play a significant role in astrophysical chain reactions. Thus, it is necessary to determine their structure and properties.

Halo Nucleus

It has been observed that some nuclei have one or more valence nucleons present outside the core at large distances. Classically these systems should be unstable, but Quantum mechanically there exist finite probability of finding nucleons at such distances. These nuclei have a stable and nearly inert core surrounded by loosely bound one or more nucleons. The outer nucleons form a halo around the stable core and are easily separated during an interaction. This type of nucleus is called **halo nucleus**, the one with valence neutrons (protons) is termed as the neutron (proton) halo. The neutron halos are relatively more stable than proton halos due to Coulomb repulsion between outer proton and positively charged core.

The examples of neutron halo are ^{11}Be, ^{14}B and ^{19}C with one neutron whereas ^{6}H, ^{11}Li, ^{14}Be and ^{17}B with two neutrons. The examples of proton halo are ^{8}B, ^{17}Ne, ^{20}Mg and $^{26,27,28}P$. ^{11}Li has two neutrons forming the halo around the core which is similar to ^{9}Li. The properties of the core of ^{11}Li are same as that of ^{9}Li. The stability of ^{11}Li was the mystery for very long time because if we remove one neutron from the halo of ^{11}Li, the other halo neutron also leaves the nucleus resulting in ^{9}Li. It becomes more mysterious with the fact that ^{10}Li does not exist in nature. Thus, ^{11}Li is a three body system in which the core and two neutron form stable system and no two bodies are in a direct bound state. If we disturb one body, the whole system becomes unstable. ^{11}Li is analogous to the Borromean Rings, which is a system of three rings where if one ring is removed then other two rings will also get unlinked.

The halo nucleus shows long density tail of Halo nucleons outside the core. According to the Heisenberg uncertainty principle, the large spatial distribution should result in narrow momentum distribution. The experimentally measured momentum distribution

of halo nucleus was found to be extremely narrow which supports the fact that halo nuclei have unusually large spatial distribution.

In this project, we have analysed the structure of ^{37}Mg which is the most neutron-rich bound isotope of Mg. ^{37}Mg is a very loosely bound system with one neutron removal energy as low as 0.16 ± 0.68 MeV. Thus, it is a promising candidate of nucleus having one-neutron halo structure.

Coupled Channel Equation

In the case of deformation, the coupling between various states of different angular momentum results in coupled channel potential. In this report, we have considered axially symmetric quadrupole deformed Woods-Saxon potential without spin-orbit term [1].

$$V(r_1) = V_{ws}(r_1) - \beta_2 k(r_1) Y_2^0(\hat{r}_1), \tag{1.3}$$

where,

$$V_{ws} = V_{ws}^0 f(r_1), \tag{1.4}$$

$$f(r_1) = \frac{1}{1 + \exp\left(\frac{r_1 - R}{a_0}\right)}, \tag{1.5}$$

$$R = r_0 A^{1/3}, \tag{1.6}$$

$$k(r_1) = R V_{ws}^0 \frac{df(r_1)}{dr_1}, \tag{1.7}$$

$$\tag{1.8}$$

and V_{ws}^0 = depth of the potential, r_0 = radius, a_0 = diffusion parameter, and β_2 = quadrupole deformation parameter. The radial Equation with the above deformed potential becomes coupled channel as

$$\left\{ \frac{d^2}{dr_1^2} - \frac{l(l+1)}{r_1^2} + \frac{2\mu}{\hbar^2}(E + V_{ws}^0 f(r_1)) \right\} u_{lm}(r_1) =$$
$$- \frac{2\mu}{\hbar^2} \sum_{l'} \langle Y_l^m(\hat{r}_1)| \beta_2 R V_{ws}^0 \frac{df(r_1)}{dr_1} Y_2^0(\hat{r}_1) |Y_{l'}^m(\hat{r}_1)\rangle u_{l'm}(r_1), \tag{1.9}$$

where $u_{l'm}(r_1)$ is the radial wave function of the projectile.

Chapter 2

R-matrix Theory

The R-matrix theory is a powerful tool of quantum physics proposed by Wigner and Eisenbud who simplified the original idea of Kapur and Peierls. Initially, R-matrix theory was used to describe resonances in nuclear reactions but later it was also developed to solve coupled channel Schroedinger equations. The R-matrix Method was developed in two directions: one is phenomenological R-matrix, and other is calculable R-matrix. The phenomenological R-matrix theory is used to parametrize various types of cross-sections. The calculable R-matrix theory is used to solve Schroedinger equation in atomic and nuclear physics. In our case, we will be dealing with calculable R-matrix.

Calculable R-matrix

Consider a scattering with potential differing from Coulomb potential by short range term.

$$V(r) \xrightarrow[r \to \infty]{} V_c(r) = \frac{Z_1 Z_2 e^2}{r} \tag{2.1}$$

In R-matrix method, we divide the configuration space into two regions: **internal region** and **external regions**. A parameter **channel radius** defines the boundary between the two regions.

In the external region, the wave function is approximated by the asymptotic form where the only phase is unknown. In the internal region, complete interaction is considered, and the system is confined. The wave function is expanded over the finite square-integrable basis. In our case, we will be using Lagrange basis. Both these forms of wave functions are equated at the channel radius to get the phase shift. The R-matrix is defined as the inverse of logarithmic derivative of the internal wave function at the channel radius.

Consider a scattering where a system leads to various channels which are represented by the orthonormal state vectors $|c\rangle$. A energy E, the total wave function [3] of the system

is expanded on the basis of $|c\rangle$ as

$$\Psi = \sum_c |c\rangle\, r^{-1} u_c(r) \tag{2.2}$$

i.e. all channels can be approximately described the same radial coordinate r. The Schroedinger equation for the system

$$(H - E)\Psi = 0 \tag{2.3}$$

can be written as a system of coupled equations with respect to the unknown radial functions $u_c(r)$,

$$(T_c - E)u_c + \sum_{c'} V_{cc'} u_{c'} = 0 \tag{2.4}$$

where $V_{cc'}$ is the coupled channel potential which also includes possible centrifugal term $\hbar^2 l_c(l_c+1)/2\mu_c r^2$ with l_c as the orbital angular momentum of channel c.. T_c is the kinetic energy of the system is

$$T_c = -\frac{\hbar^2}{2\mu_c}\frac{d^2}{dr^2}, \tag{2.5}$$

where μ_c is the reduced mass of the channel c. The coupled channel potential includes the threshold energy E_{Tc} at channel c and has asymptotic form

$$V(r) \xrightarrow[r\to\infty]{} \left(E_{Tc} + \frac{Z_{1c}Z_{2c}e^2}{r}\right)\delta_{cc'}, \tag{2.6}$$

where $Z_{1c}e$ and $Z_{2c}e$ are the charges of the nuclei in this channel. The coupling potentials are assumed to be short-ranged whose effect is taken into account in the internal region. The relative energy, wave-number, velocity and the Sommerfeld parameter in channel c are denoted as $E_c = E - E_{Tc}$, k_c, v_c and η_c respectively.

The wave function in external region is approximated by its asymptotic form as

$$u_c \xrightarrow[r\to\infty]{} v_c^{-1/2}[\delta_{ci}I_c(k_c r) - U_{ci}O_c(k_c r)], \tag{2.7}$$

where the subscript i represents the initial channel. We need to find the collision matrix $U_{cc'}$ through this asymptotic behaviour of bound solutions. The functions I_c and O_c are ingoing and outgoing Coulomb wave functions which depend on the energy E through k_c and η_c and on the orbital momentum l_c.

In R-matrix method, the configuration space in divided into two regions: internal region and the external region, the boundary is defined by the channel radius, a which is assumed to be same for all channels.

The Bloch operator

The Hamiltonian H_c is not Hermitian over the internal region $(0, a)$,

$$\int_0^a f(r) H_c g(r) dr \neq \int_0^a g(r) H_c f(r) dr, \tag{2.8}$$

where $f(r)$ and $g(r)$ are some eigenfunctions of Hamiltonian H_c. We find that the difference between the two terms is

$$\int_0^a f(r) H_c g(r) dr - \int_0^a g(r) H_c f(r) dr = \frac{\hbar^2}{2\mu} \left(f'(a) g(a) - f(a) g'(a) \right), \tag{2.9}$$

where we have used the form of H_c as

$$H_c = -\frac{\hbar^2}{2\mu} \left(\frac{d^2}{dr^2} - \frac{l(l+1)}{r^2} + \sum_{c'} V_{cc'}(r) \right), \tag{2.10}$$

This problem was solved elegantly by the introduction of Bloch surface operator:

$$\mathcal{L} = \sum_c |c\rangle \, \mathcal{L}_c \, \langle c| , \tag{2.11}$$

with

$$\mathcal{L}_c = \frac{\hbar^2}{2\mu} \delta(r - a) \left(\frac{d}{dr} - \frac{B_c}{r} \right), \tag{2.12}$$

where B_c is a boundary parameter, assumed here to be real. This operator vanishes everywhere except at $r = a$. The operator $H_c + \mathcal{L}_c$ is Hermitian over (0,a),

$$\int_0^a f(r) (H_c + \mathcal{L}_c) g(r) dr = \int_0^a g(r) (H_c + \mathcal{L}_c) f(r) dr, \tag{2.13}$$

because

$$\int_0^a f(r) \mathcal{L}_c g(r) dr - \int_0^a g(r) \mathcal{L}_c f(r) dr = -\frac{\hbar^2}{2\mu} \left(f'(a) g(a) - f(a) g'(a) \right) \tag{2.14}$$

The addition of Bloch Surface operator on both side of equation (2.4) results in Bloch-Schroedinger system of equations

$$(T_c + \mathcal{L}_c - E) u_c + \sum_{c'} V_{cc'} u_{c'} = \mathcal{L}_c u_c \tag{2.15}$$

In the external region, the wave function is approximated by its asymptotic form, hence, u_c in the R.H.S. of Equation (2.15) is replaced by Equation (2.7)

$$(T_c + \mathcal{L}_c - E) u_c^{int} + \sum_{c'} V_{cc'} u_{c'}^{int} = \mathcal{L}_c v_c^{-1/2} [\delta_{ci} I_c(k_c r) - U_{ci} O_c(k_c r)]. \tag{2.16}$$

In the internal region, the wave function u_c^{int} is expanded in some basis. We will be using Lagrange basis which is described in the next section.

6

Lagrange basis and Lagrange mesh

In the internal region, the radial wave function is expanded over a Lagrange basis,

$$u_c^{int}(r) = \sum_{n=1}^{N} A_{cn} f_n(r).$$

$$(2.17)$$

A Lagrange basis is a set of N functions $f_n(x)$ associated with a Lagrange mesh of N points ax_n on the interval $[0, a]$. The x_n are zeros of the shifted Legendre polynomial $P_N(2x - 1)$. The Lagrange functions are continuous and indefinitely differentiable

$$f_n(r) = (-1)^n a^{-1/2} \sqrt{\frac{1 - x_n}{x_n}} \frac{r P_N[2(r/a) - 1]}{r - ax_n}.$$

$$(2.18)$$

They satisfy the Lagrange conditions

$$f_{n'}(ax_n) = (a\lambda_n)^{-1/2} \delta_{nn'},$$

$$(2.19)$$

i.e. each $f_{n'}$ vanishes at all mesh points ax_n, except at $ax_{n'}$. The coefficients λ_n are the weights associated with a Gauss-Legendre quadrature approximation for the $[0, 1]$ interval

$$\int_0^1 g(x)dx \approx \sum_{n=1}^{N} \lambda_n g(x_n).$$

$$(2.20)$$

The weights λ_n are equal to the traditional Gauss-Legendre weights for the $[-1, +1]$ interval, divided by 2.

The Lagrange functions (2.18) are not orthogonal but, because of the Lagrange conditions (2.19), they are approximately orthogonal at the Gauss approximation (2.20),

$$\int_0^a f_n(r) f_{n'}(r)dr \approx \delta_{nn'}.$$

$$(2.21)$$

Bound states

The bound state of the system (2.4) or (2.16) can be calculated using the Lagrange-mesh technique. The energy E_c are all negative for an energy E below all thresholds. The asymptotic form of the function u_c in channel c is proportional to a Whittaker function $W_c(\kappa_c r)$ [9], which depends on l_c, $\kappa_c = (-2\mu_c E_c/\hbar^2)^{1/2}$ and the corresponding $\eta_c = Z_1 Z_2 \alpha (\mu_c c^2/2E)^{1/2}$

$$u_c^{ext} = D_c W_{-\eta, l_c+1/2}(2\kappa_c r)$$

$$(2.22)$$

where D_c is constant specifying amplitude for channel c. The expansion over Lagrange basis (2.17), in equation (2.16) results in

$$\sum_{n'=1}^{N} \left((T_c + \mathcal{L}_c - E)A_{cn'} f_{n'}(r) + \sum_{c'} V_{cc'} A_{c'n'} f_{n'}(r) \right) = \mathcal{L}_c u_c^{ext}.$$

$$(2.23)$$

Now taking projection of (2.23) on $f_n(r)$,

$$\sum_{c'n'} \int f_n(r)[\delta_{cc'}(T_c + \mathcal{L}_c - E) + V_{cc'}]A_{c'n'}f_{n'}(r)dr = \int f_n(r)\mathcal{L}_c u_c^{ext}dr. \tag{2.24}$$

If we choose

$$B_c = 2\kappa_c a \frac{W'_{-\eta,l_c+1/2}(2\kappa_c a)}{W_{-\eta,l_c+1/2}(2\kappa_c a)}, \tag{2.25}$$

the R.H.S. of (2.24) vanishes, i.e.

$$\int f_n(r)\mathcal{L}_c u_c^{ext}dr = \frac{\hbar^2}{2\mu_c} \int \delta(r-a)\left(\frac{du_c^{ext}}{dr} - \frac{B_c u_c^{ext}}{r}\right)dr \tag{2.26}$$

$$= \frac{\hbar^2}{2\mu_c} \int \left(D_c W'_c 2\kappa_c - \frac{B_c D_c W_c}{a}\right)dr \tag{2.27}$$

$$= \frac{\hbar^2}{2\mu_c a} \int D_c W_c \left(\frac{W'_c}{W_c} 2\kappa_c a - B_c\right)dr \tag{2.28}$$

$$= 0, \tag{2.29}$$

where we have used chosen form of B_c (2.25). Now for this choice of B_c (2.25), the equation (2.24) becomes

$$\sum_{c'n'}[C_{cn,c'n'} - E\delta_{cc'}\delta_{nn'}]A_{c'n'} = 0, \tag{2.30}$$

where we have used the orthogonality relation of Lagrange functions (2.21). The elements of the symmetric matrix C are defined as

$$C_{cn,c'n'} = \int_0^a f_n(r)[\delta_{cc'}(T_c + \mathcal{L}_c) + V_{cc'}]f_{n'}(r)dr. \tag{2.31}$$

The matrix elements of Bloch operator are

$$\int_0^a f_n(r)\mathcal{L}_c f_{n'}(r)dr = \frac{\hbar^2}{2\mu_c a}f_n(a)[af'_{n'}(a) - B_c f_{n'}(a)], \tag{2.32}$$

where f'_n is the derivative of f_n with respect to r. The potential matrix only have diagonal elements with respect to n and n'

$$\int_0^a f_n(r)V_{cc'}(r)f_{n'}(r)dr \approx V_{cc'}(ax_n)\delta_{nn'}. \tag{2.33}$$

The Kinetic matrix is diagonal with respect to channel index c and its elements are given by

$$\int_0^a f_n(r)T_c f_{n'}(r)dr = -\frac{\hbar^2}{2\mu_c}(a\lambda_n)^{1/2}f''_{n'}(ax_n). \tag{2.34}$$

8

The explicit forms of $f_n(a)$, $f'_n(a)$ and $f''_{n'}(ax_n)$ are given in Appendix A.

At the Gauss approximation, the matrix $\boldsymbol{C}$ is a real and symmetric matrix. The eigenvalues of $\boldsymbol{C}$ can easily be calculated using a standard routine (Appendix B). The value of B_c and hence $\boldsymbol{C}$ matrix depends on the bound state energy. Hence, we will consider $B_c = 0$ and will find eigenvalue for this assumed value of B_c. Then we will use this new eigenvalue to calculate B_c and will iterate. The convergence occurs within few iterations for all bound state energies.

Multichannel R-matrix

We consider that E is larger than all threshold energies, i.e. all channels are open. We will choose $B_c = 0$ for all open channels. After taking projection of the Bloch Schroedinger system on a basis function $f_n(r)$ (2.24), we obtain

$$\sum_{c'n'}[C_{cn,c'n'} - E\delta_{cc'}\delta_{nn'}]A_{c'n'} = \frac{\hbar^2 k_c}{2\mu_c\sqrt{v_c}}f_n(a)[\delta_{ci}I'_c(k_ca) - U_{ci}O'_c(k_ca)]. \tag{2.35}$$

Solving the system of equations (2.35) for A_{cn} provides with (2.17) the radial functions

$$u_c(r) = \sum_{c'} \frac{\hbar^2 k_{c'}}{2\mu_{c'}\sqrt{v_{c'}}}[\delta_{c'c}I'_{c'}(k_{c'}a) - U_{c'c}O'_{c'}(k_{c'}a)]$$

$$\times \sum_{n,n'=1}^{N} f_n(r)(\boldsymbol{C} - E\boldsymbol{I})^{-1}_{cn,c'n'}f_{n'}(a), \tag{2.36}$$

where $\boldsymbol{I}$ is a unit matrix. The function u_c in (2.36) still depends on the unknown collision matrix $\boldsymbol{U}$.

The R-matrix at energy E is defined as the inverse of logarithmic derivative of the radial wave function at the boundary between the two regions. We choose it symmetric and adimensional under the form

$$R_{cc'} = \frac{\hbar^2}{2\sqrt{\mu_c\mu'_c}a} \sum_{n,n'=1}^{N} f_n(a)(\boldsymbol{C} - E\boldsymbol{I})^{-1}_{cn,c'n'}f_{n'}(a). \tag{2.37}$$

Now, we define $\boldsymbol{Z}$ matrix as

$$Z_{cc'} = (k_{c'}a)^{-1/2}[\delta_{cc'}O_c(k_ca) - k_{c'}aR_{cc'}O'_{c'}(k_{c'}a)], \tag{2.38}$$

and equating at channel radius an expression (2.36) with its asymptotic form (2.7) provides the unitary and symmetric collision matrix

$$\boldsymbol{U} = \boldsymbol{Z}^{-1}\boldsymbol{Z}^*. \tag{2.39}$$

The above analysis has been done assuming all channels are open. Now, we will include the closed channels in which E is less than the threshold energy. Let us represent open channels by c and closed channels by $\bar{c}$. The value of B_c can be chosen according to Equation (2.25) for closed channels and $B_c = 0$ for open channels. The definition of the R matrix must be modified by first eliminating the coefficients $A_{\bar{c}n}$ which corresponds to closed channels [5]. $\boldsymbol{C}$ matrix will be replaced by a smaller open-channels matrix $\tilde{\boldsymbol{C}}$ which has following elements:

$$\widetilde{C}_{cn,c'n'} = C_{cn,c'n'} - \sum_{\bar{c}\bar{c}'} V_{c\bar{c}}(ax_n)(\bar{\boldsymbol{C}} - E\bar{\boldsymbol{I}})^{-1}_{\bar{c}n,\bar{c}'n'} V_{\bar{c}'c'}(ax_{n'}), \tag{2.40}$$

where $\bar{\boldsymbol{C}}$ is the restriction of the full matrix to closed channels. The dimension of unit matrix $\bar{\boldsymbol{I}}$ is same as that of $\bar{\boldsymbol{C}}$.

Chapter 3

Bound State Energies

In this chapter, we have described the algorithm to get bound state energies. As outlined in the previous chapter, the closed channels have threshold energies more than E and E_c are negative for these channels. We have calculated E_c using method described in section 2.4. First, we calculated the $\boldsymbol{C}$ matrix which involved the calculation of potential matrix $\boldsymbol{V}$ and Lagrange functions. The calculation of eigenvalues of $\boldsymbol{C}$ matrix required choosing $B_c = 0$ and within a few iterations, we got convergence.

Potential matrix

The Schrodinger equation, we are dealing with, contains deformed Woods-Saxon potential

$$
\begin{aligned}
&\left\{ \frac{d^2}{dr_1^2} - \frac{l(l+1)}{r_1^2} + \frac{2\mu}{\hbar^2}(E + V_{ws}^0 f(r_1)) \right\} u_{lm}(r_1) = \\
&-\frac{2\mu}{\hbar^2} \sum_{l'} \langle Y_l^m(\hat{r}_1) | \beta_2 R V_{ws}^0 \frac{df(r_1)}{dr_1} Y_2^0(\hat{r}_1) | Y_{l'}^m(\hat{r}_1) \rangle u_{l'm}(r_1),
\end{aligned}
\tag{3.1}
$$

where,

$$
f(r_1) = \frac{1}{1 + \exp\left(\frac{r_1 - R}{a_0}\right)}
\tag{3.2}
$$

$$
R = r_0 A^{1/3},
\tag{3.3}
$$

with r_0, a_0 and β_2 as radius, diffusion parameter, and quadrupole deformation parameter respectively. Comparing equation (3.1) with equation (2.4), we get $V_{ll'}$ as

$$
\begin{aligned}
V_{ll'} = &\left(\frac{\hbar^2}{2\mu} \frac{l(l+1)}{r_1^2} - V_{ws}^0 f(r_1) \right) \delta_{ll'} \\
&- \langle Y_l^m(\hat{r}_1) | \beta_2 R V_{ws}^0 \frac{df(r_1)}{dr_1} Y_2^0(\hat{r}_1) | Y_{l'}^m(\hat{r}_1) \rangle
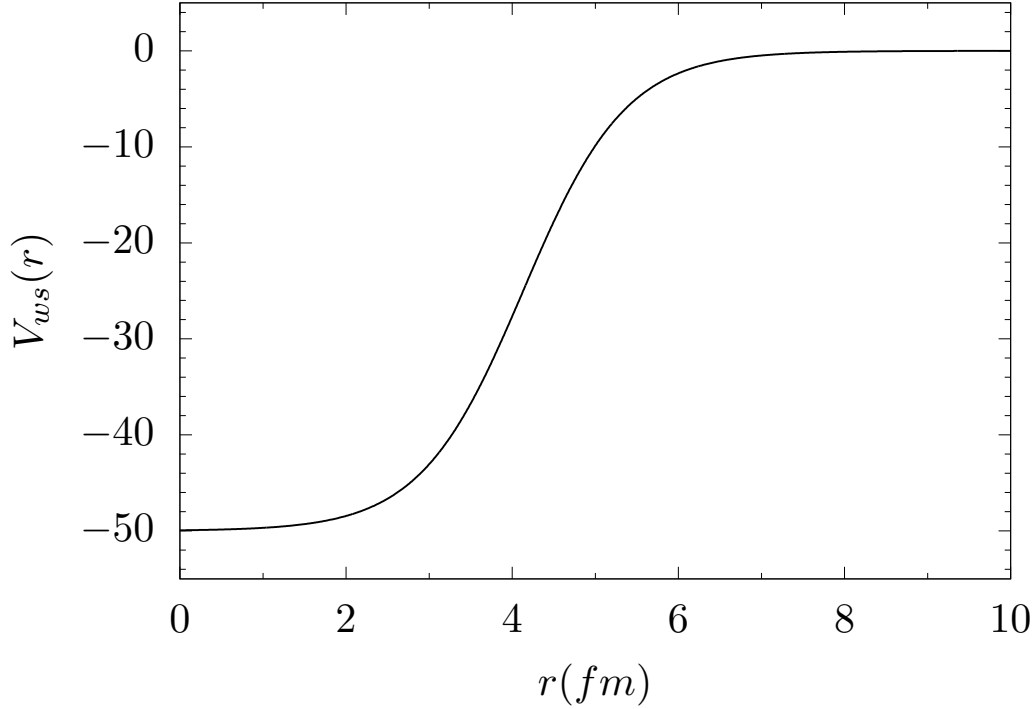\end{aligned}
\tag{3.4}
$$

11

Figure 3.1: Woods-Saxon potential for $V_{ws}^0 = 50$ MeV, $a_0 = 0.62$ fm, $A = 37$ and $r_0 = 1.24$ fm.

where l and l' represent c and c' respectively.

The first term in the potential matrix $V_{ll'}$ is trivial. We started with the expression for Woods-Saxon potential

$$V_{ws}(r) = -V_{ws}^0 \frac{1}{1 + \exp\left(\frac{r-R}{a_0}\right)}, \tag{3.5}$$

where V_{ws}^0 is the depth of Woods-Saxon potential. We have plotted $V_{ws}(r)$ for $V_{ws}^0 = 50$ MeV, $a_0 = 0.62$ fm, $A = 37$ and $r_0 = 1.24$ fm as shown in Figure 3.1. The potential depth V_{ws}^0 will be chosen such that the bound state energies correspond to the experimental measurements.

The first two terms in equation (3.4) indicate the potential without any deformation i.e. $\beta_2 = 0$. We have plotted the potential $V_l(r)$ in Figure 3.2 which is the potential without deformation

$$V_l = \frac{\hbar^2}{2\mu} \frac{l(l+1)}{r_1^2} - V_{ws}^0 f(r_1). \tag{3.6}$$

The deformation part of the potential is the product of two terms: $-\beta_2 R V_{ws}^0 \frac{df(r_1)}{dr_1}$ and $\langle Y_l^m(\hat{r}_1)| Y_2^0(\hat{r}_1) |Y_{l'}^m(\hat{r}_1)\rangle$. The first term is just the derivative of Woods-Saxon potential
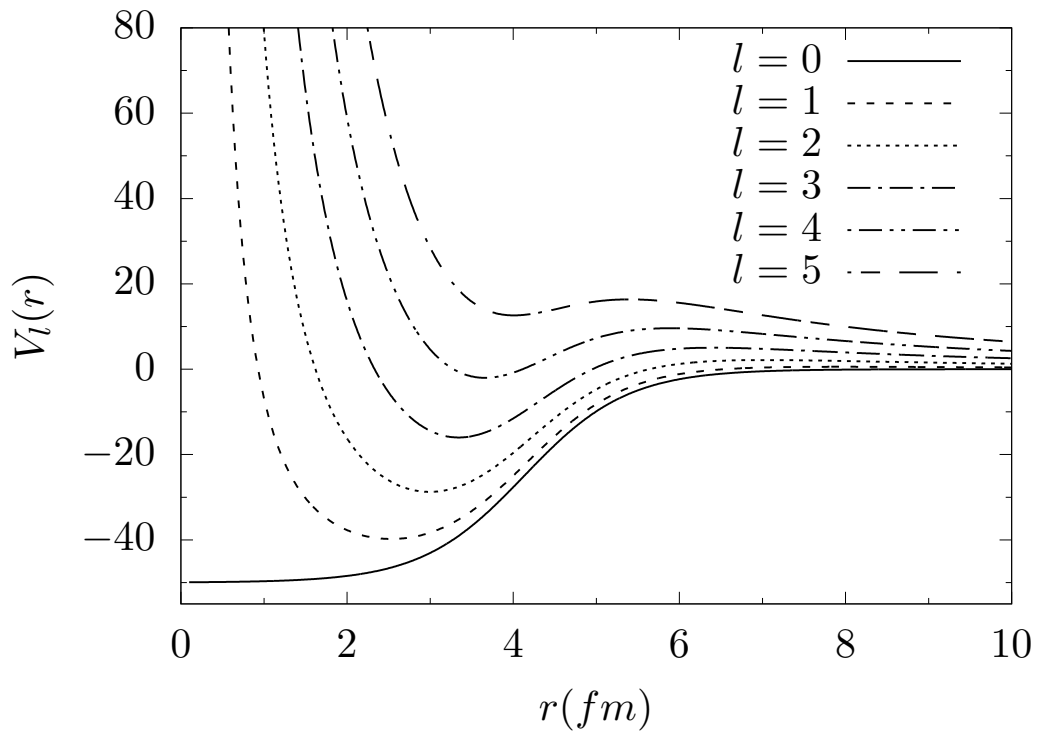
12

Figure 3.2: Potential without any deformation for $V_{ws}^0 = 50$ MeV, $a_0 = 0.62$ fm, $A = 37$, $\mu = 906.3$ MeV and $r_0 = 1.24$ fm.
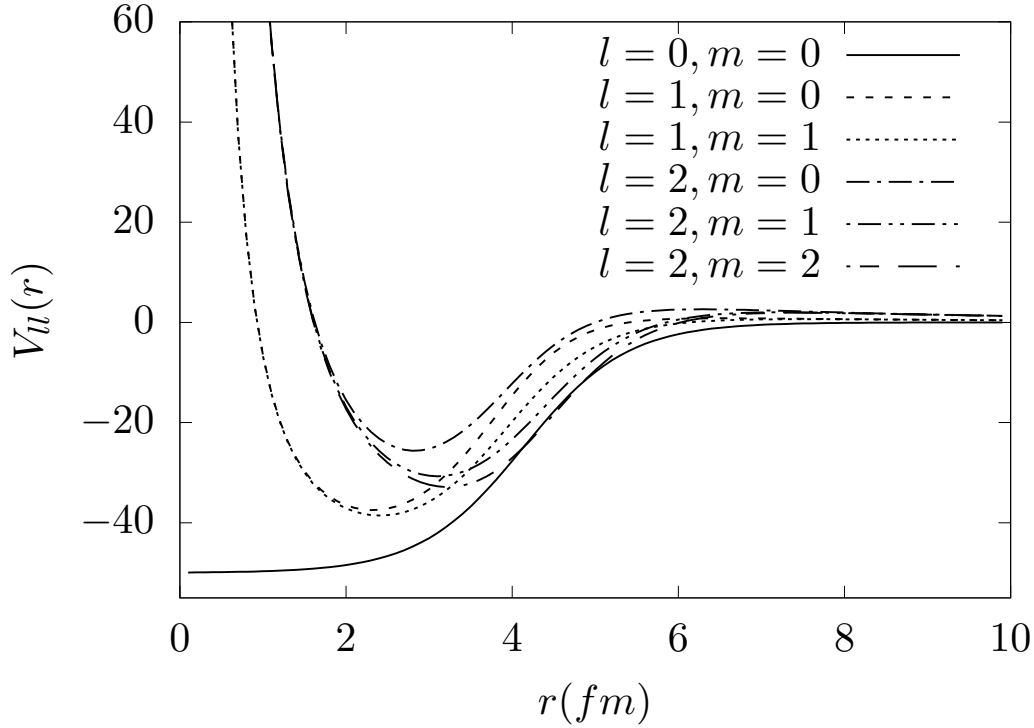
Figure 3.3: Potential with deformation parameter $\beta_2 = 0.5, V_{ws}^0 = 50$ MeV, $a_0 = 0.62$ fm, $A = 37, \mu = 906.3$ MeV and $r_0 = 1.24$ fm.

multiplied by the radius of nucleus and deformation parameter. The second term contains the spherical harmonics which can be expressed in terms of Wigner 3j symbols as

$$
\langle Y_l^m(\hat{r}_1)| Y_2^0(\hat{r}_1) |Y_{l'}^m(\hat{r}_1)\rangle = \sqrt{\frac{(2l_1 + 1)(2l_2 + 1)(2l_3 + 1)}{4\pi}}
$$
$$
\times \begin{pmatrix} l & 2 & l' \\ 0 & 0 & 0 \end{pmatrix} \begin{pmatrix} l & 2 & l' \\ m & 0 & m \end{pmatrix}.
\tag{3.7}
$$

The Wigner 3j symbols can be calculated using Racah formula, the standard subroutine can also be used for Wigner 3j symbol (Appendix B). We have plotted the potential for $l = l'$ and $\beta_2 = 0.5$ in Figure 3.3 which shows the effect of deformation on potential (3.4) for various values of m, the projection of l.

In the calculation of $\boldsymbol{C}$ matrix, the elements of $\boldsymbol{V}$ matrix (2.33) are calculated only at Lagrange mesh points ax_n

$$
\int_0^a f_n(r)V_{cc'}(r)f_{n'}(r)dr \approx V_{cc'}(ax_n)\delta_{nn'},
\tag{3.8}
$$

where a and x_n are boundary parameter and zeros of the Gauss-Legendre quadrature.

14

Kinetic matrix

The elements of kinetic matrix require $f_n''(ax_n)$ (2.32) which is given in Appendix A

$$\int_0^a f_n(r) T_c f_{n'}(r) dr = -\frac{\hbar^2}{2\mu_c}(a\lambda_n)^{1/2} f_{n'}''(ax_n),\tag{3.9}$$

where, x_n are zeros of the Gauss-Legendre quadrature which can be obtained from a standard routine (Appendix B). The kinetic matrix is diagonal with respect to the channel index c.

Bloch matrix

The elements of Bloch matrix are non-zero only at boundary, i.e. $r = a$

$$\int_0^a f_n(r) \mathcal{L}_c f_{n'}(r) dr = \frac{\hbar^2}{2\mu_c a} f_n(a)[af_{n'}'(a) - B_c f_{n'}(a)],\tag{3.10}$$

where $f_n(a)$ and $f_n'(a)$ are Lagrange function and derivative of the Lagrange function with respect to r at $r = a$. The expressions for $f_n(a)$ and $f_n'(a)$ are given in Appendix A which require zeros of the Gauss-Legendre quadrature.

For closed channels, the boundary parameter B_c depends on l_c, κ_c and η_c (2.22) through Whittaker function $W_c(2\kappa_c r)$

$$B_c = 2\kappa_c a \frac{W'_{-\eta,l_c+1/2}(2\kappa_c a)}{W_{-\eta,l_c+1/2}(2\kappa_c a)},\tag{3.11}$$

where $W_c'(2\kappa_c r)$ is derivative of $W_c(2\kappa_c r)$ at $2\kappa_c a$. The Whittaker function $W_c(2\kappa_c r)$ can be obtained using a standard routine (Appendix B).

C matrix

The elements of $\boldsymbol{C}$ matrix can be obtained from the elements of potential matrix, kinetic matrix and Bloch matrix (2.31) as

$$
\begin{aligned}
C_{cn,c'n'} = \frac{\hbar^2}{2\mu_c a} &\left(-a(a\lambda_n)^{1/2} f_{n'}''(ax_n) + f_n(a)[af_{n'}'(a) - B_c f_{n'}(a)]\right) \delta_{cc'} \\
&+ V_{cc'}(ax_n)\delta_{nn'}
\end{aligned}\tag{3.12}
$$

where B_c is unknown because B_c depends on eigenvalue E_c. We take the initial value as $B_c = 0$ and calculate the $\boldsymbol{C}$ matrix. The $\boldsymbol{C}$ matrix is real and symmetric matrix whose eigenvalues can be obtained using a standard routine (Appendix B). The eigenvalues have one negative energy that is bound state energy. We use this negative energy as

Table 3.1: Eigen Values of C matrix for non-deformed Wood-Saxon Potential with $V_{ws}^0 = 45$ MeV, $r_0 = 1.26$ fm, $a_0 = 0.62$ fm for the case of ^{37}Mg.

S. No.	Eigenvalue
1	6064.907214
2	1030.076478
3	231.378992
4	-22.268603
5	-0.594533
6	4.475110
7	36.110060
8	60.178550
9	114.719343
10	18.326637

first approximation of eigenvalue and calculate B_c as given in Equation (3.11). Now, we calculate C matrix using this new approximation of B_c and iterate the above step to obtain more approximate eigenvalues. The convergence occurs within few iterations. Using this approach, we calculate E_c for all channels.

Eigenvalues of C matrix

The C matrix was calculated for deformed Wood-Saxon potential as described in Section 3.1. The parameter used for deformed Wood-Saxon potential are $V_{ws}^0 = 45$ MeV, $r_0 = 1.26$ fm, $a_0 = 0.62$ fm and deformation parameter, $\beta_2 = 0$. We first calculated the bound state energy of ^{37}Mg with $2P$ as a ground state in the absence of deformation. Our equation (3.1) considers two body interaction where one nucleon interact with the core consisting of 36 Nucleons. The reduced mass μ is calculated as

$$\mu = \frac{m_1 m_2}{m_1 + m_2} = 938.92 \times \frac{36}{37} \text{ MeV}. \tag{3.13}$$

The value of Planck's Constant is taken as $\hbar = 197.32697$ and $l = 1$ for the state $2P$. The Number of mesh points are taken as $N = 10$ which means the potential is calculated at 10 points only in the region $(0, a)$ where $a = 10$. The eigenvalues of C matrix was calculated using standard subroutine Mardi (Appendix B).

The eigenvalues of C matrix are listed in Table 3.1 which shows there are two negative eigenvalues, both of which are bound state energies. Since the Hamiltonian does not contain information about principle quantum number n, so the choice of $l = 1$ corresponds to both $1P$ and $2P$ states. If we increase the depth of Wood-Saxon potential, V_{ws}^0, higher P states will also get bound. Hence, -22.268 and -0.594 corresponds to 1P and 2P states of ^{37}Mg.

Table 3.2: Iteration using B_c which is function of bound state energy E_c. Non-deformed Wood-Saxon Potential with $V_{ws}^0 = 45$ MeV, $r_0 = 1.26$ fm, $a_0 = 0.62$ fm for the case of ^{37}Mg.

Iteration	Eigenvalues	
1	-22.268603	-0.594533
2	-22.268581	-0.341003
3	-22.268584	-0.365732
4	-22.268583	-0.362974
5	-22.268583	-0.363277
6	-22.268583	-0.363244
7	-22.268583	-0.363247
8	-22.268583	-0.363247
9	-22.268583	-0.363247
10	-22.268583	-0.363247

The negative eigenvalue is used to calculate B_c which defines a more approximate $\boldsymbol{C}$ matrix. We used $E_c = -0.594533$ and calculated the eigenvalues of $\boldsymbol{C}$ matrix again. We get the convergence within few iterations, the eigenvalues after each iteration are given in Table 3.2. The iterative method eventually provides us with the bound state energies, the value of B_c and $\boldsymbol{C}$ matrix which are required later in the calculation of wave functions.

The boundary parameter, a and the number of Lagrange points, N were fixed in the calculation of Table 3.1 and 3.2. The bound state energies should not depend on the choice of boundary parameter and number of Lagrange points. We calculated the bound state energies with variation in boundary parameter, a and results are given in Table 3.3. We observe that the eigenvalues are not changing significantly with a. The eigenvalues at the lower value of a are not much consistent but they become constant for a greater than 10.

We have calculated the bound state energies for the various choices of the number of mesh points. The accuracy of results increases with the increase in the number of mesh points but the larger amount of computation is required with the increase in the number of mesh points. The bound states energies calculated with various number of mesh points are given in Table 3.4. We can see that the desired accuracy is obtained with 30 points and increasing the number of points does not help in getting more accurate results instead that requires a huge amount of computation.

Determination of Depth of Wood-Saxon Potential

In the previous calculations, we have selected the depth of Wood-Saxon potential as $V_{ws}^0 = 45 MeV$. In nuclear physics, the depth of potential is different for various nuclei and can not be obtained theoretically. The bound state energies of nuclei are measured

Table 3.3: Variation in Eigenvalues with the channel radius, a for non-deformed Wood-Saxon Potential with $V_{ws}^0 = 45$ MeV, $r_0 = 1.26$ fm, $a_0 = 0.62$ fm for the case of ^{37}Mg.

N	a	Eigenvalues	
30	6.0	-22.309576	
30	8.0	-22.313414	
30	10.0	-22.313467	-0.307101
30	12.0	-22.313425	-0.314110
30	14.0	-22.313425	-0.317194
30	16.0	-22.313444	-0.318609
30	18.0	-22.313371	-0.319500
30	20.0	-22.313525	-0.319483
30	22.0	-22.313092	-0.320692
30	24.0	-22.314255	-0.315125
30	26.0	-22.312466	-0.320421
30	28.0	-22.311983	-0.322450
30	30.0	-22.316987	-0.311771

Table 3.4: Variation in eigenvalues with number of mesh points N for non-deformed Wood-Saxon Potential with $V_{ws}^0 = 45$ MeV, $r_0 = 1.26$ fm, $a_0 = 0.62$ fm for the case of ^{37}Mg.

N	a	Eigenvalues	
10	10.0	-22.268583	-0.363247
20	10.0	-22.313446	-0.307141
30	10.0	-22.313466	-0.307101
40	10.0	-22.313466	-0.307101
50	10.0	-22.313466	-0.307101

experimentally, which can be used to determine the depth of Wood-Saxon potential. We set the depth of Wood-Saxon potential such that the bound state energy becomes equal to the experimental value.

We calculated the depth of Wood-Saxon potential for ^{37}Mg which is a neutron Halo nucleus. The one-neutron separation energy of ^{37}Mg is very low because the Halo neutron is loosely bound to the core. The experimentally measured value of neutron separation energy is in the range 0.16 ± 0.68 MeV. However, the information about the ground state's spin and parity is not available. The state $2P_{3/2}$ is a promising candidate for the ground state.

The Hamiltonian in our equation (3.1) does not include the l-s coupling. Hence, the quantum number j is not defined and we take $2P$ as the ground state of ^{37}Mg. We take $l = 1$, $N = 20$, $a = 10$ and bound state energy $E_1 = -0.16$, the parameter of Wood-Saxon potential are same as taken in the previous calculations.

The depth of Wood-Saxon potential, V_{ws}^0 is determined by the iterative method, in

Table 3.5: Variation of Bound State Energies with deformation parameter β_2 for Wood-Saxon Potential with $r_0 = 1.26$ fm, $a_0 = 0.62$ fm for the case of ^{37}Mg.

β_2	V_0	l	E_l	β_2	V_0	l	E_l
0.0	44.36700	0	-32.12699	0.6	17.14900	0	-8.63691
		0	-9.08003			1	-22.96095
		1	-21.80121			1	-0.15979
		1	-0.15992			2	-3.77077
		2	-10.57405	0.7	15.59600	0	-7.41633
0.1	34.01200	0	-22.90156			1	-23.52389
		0	-3.24220			1	-0.15955
		1	-19.39239			2	-3.62139
		1	-0.15989			3	-0.10704
		2	-6.66078	0.8	14.29400	0	-6.41482
0.2	28.24300	0	-17.87784			1	-23.99877
		0	-0.86635			1	-0.15989
		1	-19.71552			2	-3.50162
		1	-0.15981			3	-0.23875
		2	-5.26889	0.9	13.18600	0	-5.58113
0.3	24.30600	0	-14.51919			1	-24.39751
		1	-20.59425			1	-0.15943
		1	-0.15984			2	-3.40104
		2	-4.60895			3	-0.34490
0.4	21.35200	0	-12.04931	1.0	12.18500	0	-4.84522
		1	-21.49359			1	-24.59994
		1	-0.15965			1	-0.12526
		2	-4.22211			2	-3.25696
0.5	19.02900	0	-10.14592			3	-0.36396
		1	-22.28817				
		1	-0.15972				
		2	-3.96204				

which we set potential to some initial value and calculate bound state energy for $2P_{3/2}$. If the calculated energy is not equal to the experimental value, then we decrease the depth of potential by a small amount and calculate the bound state energy again. We stop this iteration once we get the desired value of bound state energy. At the end of the iteration, we get the bound state energies and the depth of potential.

We have determined the depth of potential for various value of deformation parameter,β_2 where $\beta_2 = 0$ corresponds to non-deformed case. We have also listed all the bound state energies for a particular depth of potential. It is to be noted that we have selected $2P$ as the ground state of ^{37}Mg which may not be true as the deformation increase. The variation of the depth of potential with respect to deformation parameter is listed in Table 3.5.

The above calculation gives us the depth of potential for various deformations. We have also calculated the depth of potential for the non-deformed case using Lagrange mesh technique with Laguerre basis whose results can be used for comparison. This Lagrange mesh technique with Laguerre basis does not require Bloch matrix, we just have to calculate the kinetic and potential matrix element. The eigenvalue of the Hamiltonian matrix gives the bound state energies for non-deformed case. We have listed all the eigenvalues calculated using Laguerre-Lagrange mesh in Table 3.6.

In the calculation, we have set $V_{ws}^0 = 43.80520$, so that we get the bound state energy of P state as -0.16. The depth of potential required to obtain the experimental value of bound state energy is of the same order as listed in Fig3.5. We can also observe that there are two negative eigenvalues for P state, which corresponds to $1P$ and $2P$ states.

The depth of Wood-Saxon potential for the non-deformed case is also obtained using a standard routine which gives potential depth and the single particle wave function. We set the bound state energy for $2P_{3/2}$ of ^{37}Mg as -0.1600 MeV and obtained the potential depth as 43.4606 MeV. We have also set the bound state energy of $1P_{3/2}$ as -21.2803 which was obtained using R-matrix method for $V_{ws}^0 = 44.367$ MeV, we obtained $V_{ws}^0 = 43.07548$ MeV. This clearly shows that the two negative eigenvalues obtained in R-matrix method corresponds to $1P$ and $2P$ states. The depths of non-deformed Wood-Saxon potential obtained from these algorithms are listed in Table 3.7. We can see that the potential depth required to obtain the experimental value of bound state energy is of the same order.

Bound State of Deuteron

Deuteron is the smallest bound state nucleus which consists of one proton and one neutron. We have calculated the bound state energy of Deuteron using R-matrix method and Laguerre-Lagrange mesh for comparison. The potential used for Deuteron can be expressed as

$$V(r) = -V_0 \exp\left(-\alpha r^2\right), \tag{3.14}$$

Table 3.6: Bound State Energy of $2P$ state by Laguerre-Lagrange Mesh without R-matrix Method for non-deformed Wood-Saxon Potential with $V_{ws}^0 = 43.80520$ MeV, $r_0 = 1.26$ fm, $a_0 = 0.62$ fm for the case of ^{37}Mg.

S.No.	Eigenvalue
1	12050.13213
2	715.44764
3	169.34277
4	60.12403
5	-21.28013
6	-0.16001
7	35.83051
8	21.74971
9	0.74895
10	14.37334
11	9.88658
12	5.00281
13	7.00276
14	0.20692
15	3.58506
16	2.53993
17	1.76614
18	0.42968
19	1.18288
20	0.06691

Table 3.7: Depth of non-deformed Wood-Saxon potential such that Bound State Energy of $2P_{3/2}$ for ^{37}Mg is equal to -0.16 MeV. Here $r_0 = 1.26$ fm, $a_0 = 0.62$ fm.

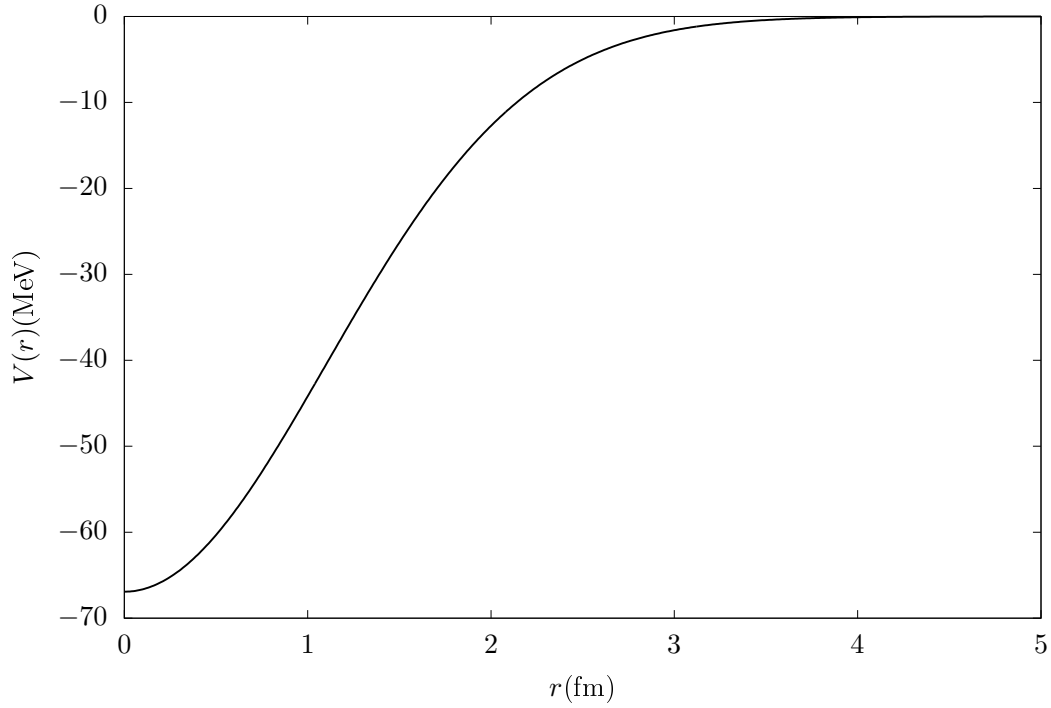| S.No.	Algorithm	V_0	Eigenvalue
1	Single Particle Wave function	43.46026	-0.16000
2	Laguerre-Lagrange Mesh	43.80520	-0.16001
3	R-Matrix Method	44.36700	-0.15992

Figure 3.4: Potential $-V_0 \exp\left(-\alpha r^2\right)$ with $V_0 = 66.92$ MeV and $\alpha = 0.415$ fm^{-2}

Table 3.8: Bound State energy of Deuteron with potential, $-V_0 \exp\left(-\alpha r^2\right)$ using R-Matrix Method with $V_0 = 66.92$ MeV and $\alpha = 0.415$ fm^{-2}

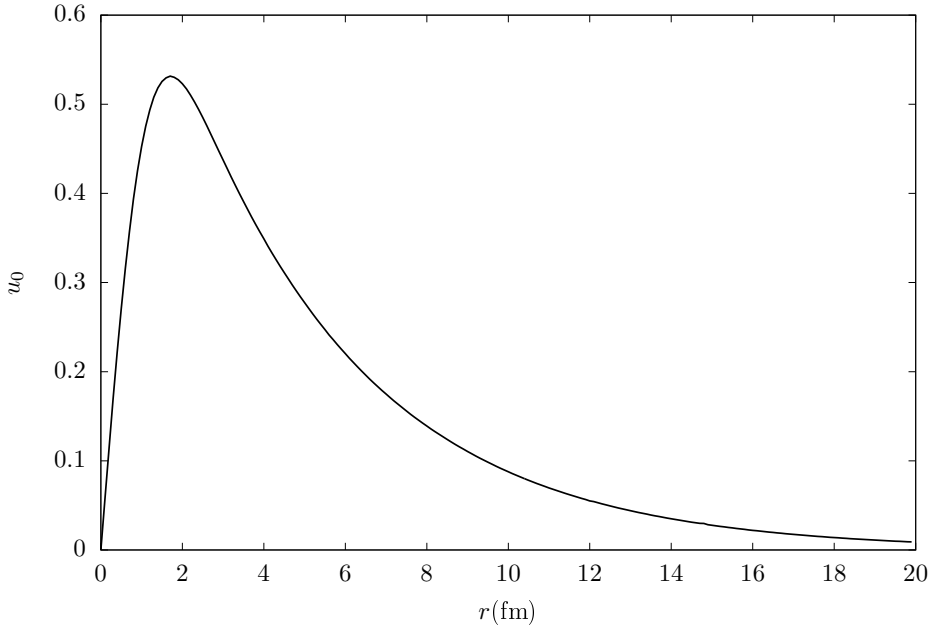| a	E
6.0	-2.19375
8.0	-2.20682
10.0	-2.21081
12.0	-2.21211
14.0	-2.21254
16.0	-2.21269
18.0	-2.21274
20.0	-2.21276
22.0	-2.21277
24.0	-2.21277
26.0	-2.21277
28.0	-2.21277
30.0	-2.21277

Figure 3.5: The bound state wave function of Deuteron for the Potential $-V_0 \exp\left(-\alpha r^2\right)$ using Laguerre-Lagrange Mesh with $V_0 = 66.92$ MeV and $\alpha = 0.415$ fm^{-2}

where $V_0 = 66.92$ MeV and $\alpha = 0.415$ fm^{-2}. The reduced mass for deuteron was taken as $\mu = 469.4592623$. The bound state energy was calculated for this potential using R-matrix method. The eigenvalue was calculated for various values of boundary parameter, a and the result is listed in Table 3.8.

We can see that the bound state energy does not change by a significant amount with the channel radius, a. The bound state energy also becomes constant for the channel radius larger than $a = 22$.

The eigenvalue is also calculated using Laguerre-Lagrange mesh technique with $N = 20$. The eigenvalues are listed in Table 3.9, in which we can see that there is one negative eigenvalue. This negative eigenvalue corresponds to the bound state energy of Deuteron. We have also calculated the wave functions for Deuteron using Laguerre-Lagrange Mesh Technique. The Figure 3.5 shows the bound state wave-function corresponding the the negative eigenvalue. The Figure 3.6 shows some of the wave-functions out of 20, the wave-function other than bound state show oscillatory behaviour because they corresponds to continuum energy states.

We have also checked the orthonormality of these wave-functions. The rms value of r is also calculated using these wave-functions which is found to be around 3.9034 fm. We have listed both eigenvalues obtained using R-matrix method and Laguerre-Lagrange mesh technique in Table 3.10.

From Table 3.10, we can compare that the result of R-matrix method is more accurate than the result of just Lagrange mesh Technique. Thus, it clearly shows that the R-matrix

23

Table 3.9: Bound State energy of Deuteron with potential, $-V_0 \exp\left(-\alpha r^2\right)$ using Laguerre-Lagrange Mesh with $V_0 = 66.92$ MeV and $\alpha = 0.415$ fm^{-2}

S.No.	Eigenvalue
1	6998.60650
2	721.78196
3	-2.19930
4	247.04743
5	123.09420
6	72.04641
7	11.34043
8	46.08855
9	31.18602
10	0.07014
11	21.85608
12	8.23441
13	15.65693
14	0.65108
15	5.94310
16	4.22337
17	2.91905
18	1.93093
19	1.18978
20	0.28382

Table 3.10: Bound State energy of Deuteron with potential, $-V_0 \exp\left(-\alpha r^2\right)$ From Various approach.

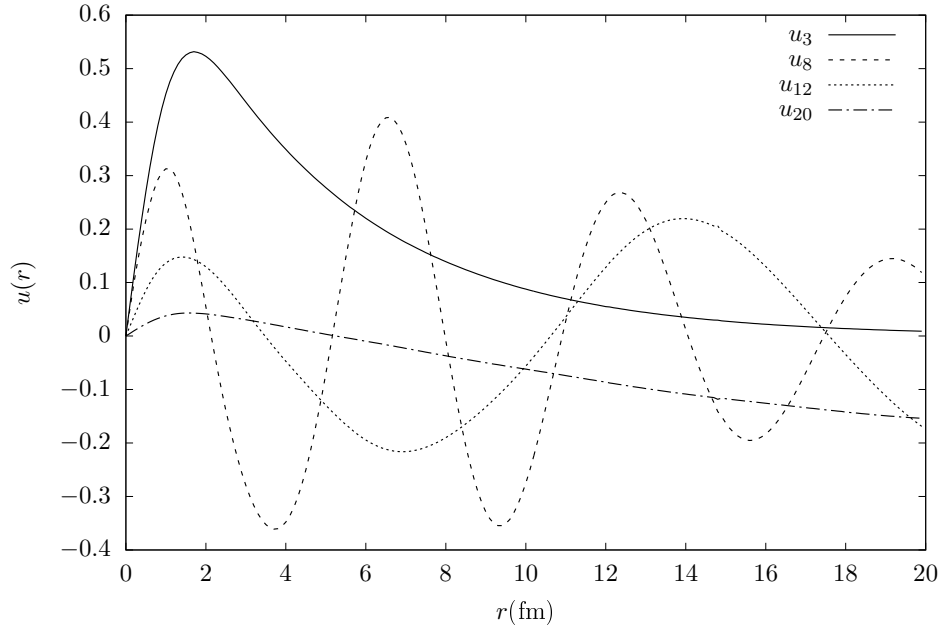| S.No.	Method	Eigen Value
1	R-Matrix Method	-2.21277
2	Laguerre-Lagrange Mesh	-2.19930
3	Experimental Value	2.224589 ± 0.000002

Figure 3.6: Some wave functions of Deuteron for the Potential $-V_0 \exp\left(-\alpha r^2\right)$ using Laguerre-Lagrange Mesh with $V_0 = 66.92$ MeV and $\alpha = 0.415$ fm^{-2}

method is more accurate than Lagrange mesh. This extra accuracy lies in the fact, in R-matrix method, we use iterations to refine the eigenvalues whereas in Lagrange mesh we find eigenvalue just once. The dependence of Whittaker function on bound state energy (2.25) ensures that we get accurate results.

The R-matrix method does not require a large number of iteration for convergence of eigenvalues, usually 5 iterations are enough if we are using 20 mesh points. We have used 10 iterations for all the previous calculations. The value of channel radius, a may have some effect on the number of iterations but using more number of mesh points compensates for that.

Chapter 4

Wave function

The calculation of bound state energy and $\boldsymbol{C}$ matrix is necessary for calculation of the wave function of the coupled system. When E is greater than threshold energy, then the channel is called open channel and we take $B_c = 0$ for those channels. For closed channels, the value of B_c is taken as the function of bound state energy, E_c through Whittaker function (2.25). We have done our calculation, considering all the channels open i.e. $B_c = 0$.

R matrix

The calculation of wave function requires $\boldsymbol{R}$ matrix (2.37) which is defined as

$$R_{cc'} = \frac{\hbar^2}{2\sqrt{\mu_c \mu_c'} a} \sum_{n,n'=1}^{N} f_n(a)(\boldsymbol{C} - E\boldsymbol{I})^{-1}_{cn,c'n'} f_{n'}(a). \tag{4.1}$$

The calculation of $\boldsymbol{R}$ matrix requires inverse of $(\boldsymbol{C} - E\boldsymbol{I})$ matrix, where $\boldsymbol{I}$ is identity matrix and E is energy. So, the calculation of this inverse matrix is straight forward. The function $f_n(a)$ are Lagrange functions given in Appendix A. Thus, $\boldsymbol{R}$ matrix can be calculated, we considered two channels which resulted in a (2×2) $\boldsymbol{R}$ matrix.

Z matrix

The calculation of $\boldsymbol{Z}$ matrix (2.38) requires computation of ingoing and outgoing Coulomb functions [8] as

$$Z_{cc'} = (k_{c'} a)^{-1/2} [\delta_{cc'} O_c(k_c a) - k_{c'} a R_{cc'} O'_{c'}(k_{c'} a)]. \tag{4.2}$$

The ingoing and outgoing function are defined in terms of Regular and Irregular Coulomb functions as

$$I_c = (G_c - iF_c) \exp(i\omega_c) \tag{4.3}$$

$$O_c = (G_c + iF_c) \exp(-i\omega_c), \tag{4.4}$$

where,

$$\omega_c = \omega_{\alpha l} = \sigma_{\alpha l} - \sigma_{\alpha 0} = \sum_{n=1}^{l} \tan^{-1}\left(\frac{\eta_\alpha}{\eta}\right). \tag{4.5}$$

In our case, neutron is neutral particle, i.e. $\eta_\alpha = 0$, hence $\omega_c = 0$. The Coulomb functions F and G can be obtained from a standard routine (Appendix B). The calculation of Coulomb Function enables us to calculate $\boldsymbol{Z}$ matrix.

Collision matrix

The Collision matrix $\boldsymbol{U}$ can be calculated from the $\boldsymbol{Z}$ matrix as

$$\boldsymbol{U} = \boldsymbol{Z}^{-1}\boldsymbol{Z}^*,. \tag{4.6}$$

where $\boldsymbol{Z}^{-1}$ and $\boldsymbol{Z}^*$ are the inverse and complex conjugate of $\boldsymbol{Z}$ matrix. The inverse of $\boldsymbol{Z}$ matrix requires a subroutine to find inverse of complex matrix (see Appendix B. Once both of these matrices are calculated, we can easily calculate collision matrix, $\boldsymbol{U}$.

Radial Wave Function

The radial wave function (2.36) requires ingoing, outgoing, collision matrix, $f_n(a)$ and $f_n(r)$ (2.18)

$$u_c(r) = \sum_{c'} \frac{\hbar^2 k_{c'}}{2\mu_{c'}\sqrt{v_{c'}}}[\delta_{c'c}I'_{c'}(k_{c'}a) - U_{c'c}O'_{c'}(k_{c'}a)]$$

$$\times \sum_{n,n'=1}^{N} f_n(r)(\boldsymbol{C} - E\boldsymbol{I})^{-1}_{cn,c'n'} f_{n'}(a). \tag{4.7}$$

The wave function depends on r only through the term

$$D_{cc'}(r) = \sum_{n,n'=1}^{N} f_n(r)(\boldsymbol{C} - E\boldsymbol{I})^{-1}_{cn,c'n'} f_{n'}(a) \tag{4.8}$$

where $f_c(r)$ is oscillatory in nature but complete summation results in the smooth curve for $c = c'$ as shown in Figure 4.1. However, the off-diagonal terms are oscillatory and have larger amplitude. Thus, the final wave function is also highly oscillatory. We are trying to rectify this problem.
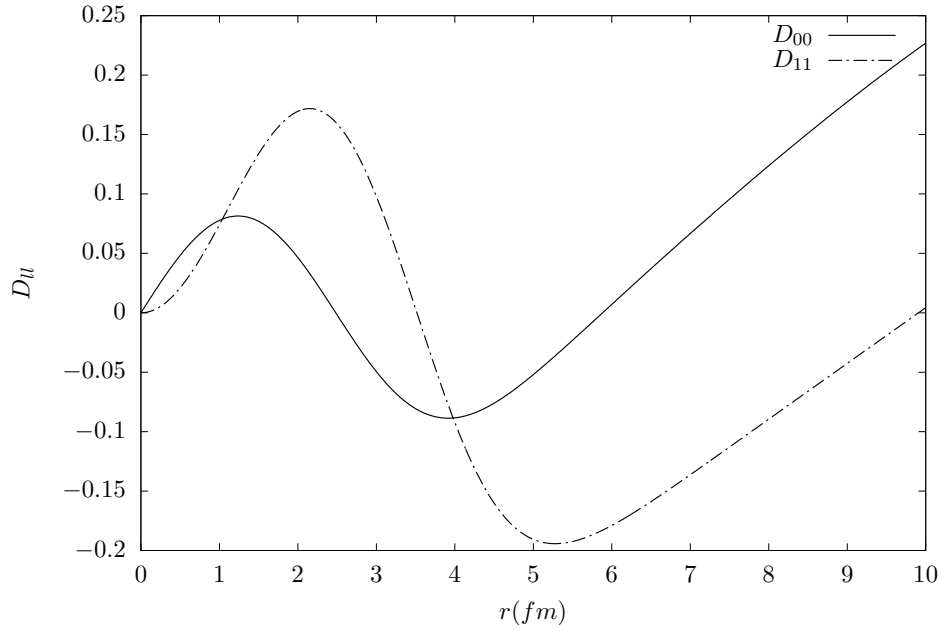
Figure 4.1: Diagonal term of $D_{ll'}$ are smooth but they have very small amplitude.
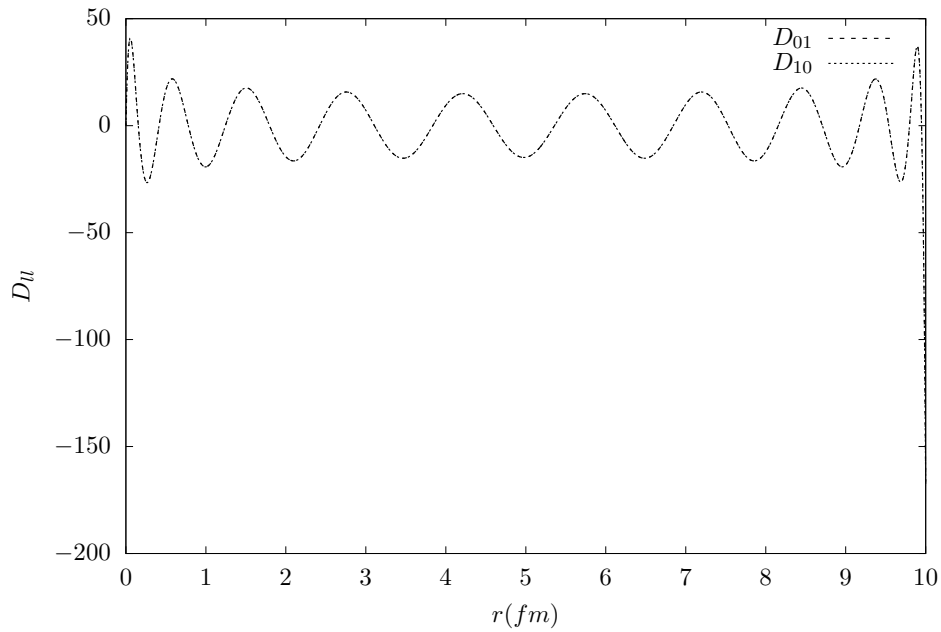

Figure 4.2: Off-diagonal term of $D_{ll'}$ are highly oscillatory in nature and they also have very large amplitude.

Chapter 5

Conclusion

In this report, we have presented the method of determination of bound-state energies in various potentials which also include deformed potentials. The R-matrix method is capable of determining the bound state energies for deformed as well as coupled channel potential.

We have compared bound state energy for ^{37}Mg and Deuteron. ^{37}Mg includes the deformed Wood -Saxon potential with coupling between various l terms. The potential can be approximated to non-deformed potential by choosing deformation parameter as $\beta_2 = 0$. The results for determination of depth of non-deformed Wood-Saxon potential were found to be in agreement with the results from other standard methods like Laguerre-Lagrange Mesh technique and Single particle wave function program. The bound state energies were also obtained for various deformation which shows that the rearrangement of states occurs as shown in Table 3.5. After some deformation, the states with higher angular momentum start acquiring lower bound states which indicate that the ground state of the system changes at higher deformation.

The bound state energy for Deuteron was found using R-matrix method and the results were found to be in agreement with experimental value as well as the value obtained from Laguerre-Lagrange mesh technique. The wave functions of Deuteron were also determined using Laguerre-Lagrange Mesh Technique.

The two important inputs in R-matrix method are channel radius, a and the number of mesh point. It is shown in the previous chapter that the value of bound-state energy is independent of the choice of channel radius and number of mesh points. The advantage of using R-matrix with Lagrange mesh is that we need to calculate potential only at mesh points. This reduces the computation requirement without any compensation for the accuracy.

The calculation for wave function is complete but the behaviour of the wave function is not satisfactory. The highly oscillatory behaviour required to be removed before we get some useful wave function.

Appendix A

Gauss-Legendre Quadrature

In this section, we have gathered the simple expressions for the calculation of various matrix elements in R-matrix method. The zeros and weights of Gauss-Legendre quadrature can be obtained from some library routine (Appendix B). The calculation of kinetic energy matrix elements (3.9) requires the simple expressions

$$a^2 f_n''(ax_n) = -(a\lambda_n)^{-1/2} \frac{N(N+1)x_n(1-x_n) - 3x_n + 1}{3x_n^2(1-x_n)^2} \tag{A.1}$$

and

$$a^2 f_{n'}''(ax_n) = -(-1)^{n+n'}(a\lambda_n)^{-1/2} \frac{x_n + x_{n'} - 2x_n^2}{x_{n'}(x_{n'} - x_n)^2} \sqrt{\frac{x_{n'}(1-x_{n'})}{x_n(1-x_n)^3}}. \tag{A.2}$$

The Bloch matrix elements can be obtained using expressions

$$f_n(a) = (-1)^n a^{-1/2}[x_n(1-x_n)]^{-1/2} \tag{A.3}$$

$$a f_n'(a) = [N^2 + N + 1 - (1-x_n)^{-1}]f_n(a). \tag{A.4}$$

The value of λ_n can be obtained using expression

$$\lambda_n = [4x_n(1-x_n)]^{-1}[P_N'(2x_n - 1)]^{-2}. \tag{A.5}$$

Appendix B

Packages

The calculation of binding energy required various standard packages. We are listing them below:

- **WITT**: Whittaker function and their derivative were calculated using this subroutine.

- **gammln**: Provides log of gamma function. We modified it to give gamma function.

- **Wig3j**: This subroutine calculates Wigner 3j symbol required in the calculation of potential matrix. This is standard routine but we made our own using Racah formula.

- **MARDI**: The eigenvalue and eigenfunction of a symmetric matrix can be calculated using this.

- **Inverse**: The inverse of a matrix can be found using this.

- **COULCC**: This is standard routine for the calculation of Coulomb Functions and their derivative.

- **CMATINV**: This standard routine provides inverse of complex matrix.

- **MATMUL**: This routine multiplies two complex matrices.

- **setmgl**: This routine provides the zeros and weights of Gauss-Legendre Quadrature.

Bibliography

[1] Shubhchintak et al., Nucl. Phys. A 939 (2015) 101.

[2] Shubhchintak, R. Chatterjee / Nucl. Phys. A 922 (2014) 99.

[3] M. Hesse et al., Nucl. Phys. A 640 (1998) 37.

[4] P Descouvemont, D Baye, Rep. Prog. Phys. 73 (2010) 036301

[5] A.M. Lane, R.G. Thomas, Rev. Modern Phys. 30 (1958) 257.

[6] P. Descouvemont, Comput. Phys. Commun. 200 (2016) 199.

[7] Sam M. Austin, George F. Bertsch, Sci. Am., 272, 6, (1995), 90.

[8] I.J. Thompson, NIST Handbook of Mathematical Functions, Cambridge University Press (2010) p. 741.

[9] A.B. Olde, Daalhuis, NIST Handbook of Mathematical Functions, Cambridge University Press (2010) p. 321.